Journal of Marine Science and Technology

Volume 27 | Issue 5 Article 6

Nonlinear Dynamic Response of a Fluid-Conveying Pipe with a Y-Type Manifold Under Different End Conditions

Xu Liang

Ti-Tao Wang

Chen-Wei Chen

Yu Deng

Yong-Du Ruan

Recommended Citation

Liang, Xu; Wang, Ti-Tao; Chen, Chen-Wei; Deng, Yu; and Ruan, Yong-Du (2019) "Nonlinear Dynamic Response of a Fluid-Conveying Pipe with a Y-Type Manifold Under Different End Conditions," *Journal of Marine Science and Technology*: Vol. 27: Iss. 5, Article 6.
DOI: 10.6119/JMST.201910_27(5).0006
Available at: https://jmstt.ntou.edu.tw/journal/vol27/iss5/6

Nonlinear Dynamic Response of a Fluid-Conveying Pipe with a Y-Type Manifold Under Different End Conditions

Acknowledgements

The authors gratefully acknowledge the financial support provided by the Fundamental Research Funds for the Central Universities (2016QNA4035), and by the National Natural Science Foundation of China (Nosd51379185, 51679214).

Journal of Marine Science and Technology, Vol. 27, No. 5, pp. 435-447 (2019)
DOI: 10.6119/JMST.201910_27(5).0006

NONLINEAR DYNAMIC RESPONSE OF A FLUID-CONVEYING PIPE WITH A Y-TYPE MANIFOLD UNDER DIFFERENT END CONDITIONS

Xu Liang*, Ti-Tao Wang, Chen-Wei Chen, Wei-Hui Wang, Yu Deng, and Yong-Du Ruan

Key words: nonlinear dynamic response, Y-type manifold, Galerkin method, Hamilton's principle.

ABSTRACT

This article addressed the discussion on the nonlinear dynamic response of a fluid-conveying pipe with a Y-type manifold under different end conditions. In which, the pipe element was regarded as an Euler-Bernoulli beam and the control volume of the flowing fluid was simplified as a jet. The governing equation of such a nonlinear dynamic problem was derived using Hamilton's principle and the momentum equation for the steady flow condition. The Galerkin method and the Runge-Kutta method with fourth-order truncation were used for solving the governing equation. To validate the numerical model, the numerical results were compared with the existing literature and showed in good agreement. In addition, parametric analyses of the nonlinear dynamic response have been done. Among which, the parameters such as the angle of the manifold, the aspect ratio, the end constraints of the pipe and the flow velocity were taken into consideration. It was concluded that : (1) the dimensionless critical flow velocity of the fluid-conveying pipe rises up significantly and the dimensionless peak deflection decreases as the angle between the central axis of pipe and manifold increases; (2) the dimensionless peak deflection of the pipe goes up as the aspect ratio increases; (3) the dimensionless peak displacement of the pipe increases with an increase in the total number of degrees of freedom at the ends; (4) when the dimensionless velocity is small, dimensionless peak deflection is insensitive to the dimensionless velocity, but when it is large, the dimensionless peak deflection rises up with the increase of the dimensionless velocity; (5) the nonlinear behavior of the pipe is mainly dominated by the first-order mode; (6) the nonlinearity of the pipe is positively correlated with the aspect ratio and the total number of degrees of freedom at the ends, and this effect is significant. However, there is a non-significant inverse correlation between the manifold angle and nonlinearity. The research results in this paper may provide reference for the engineering practice of pipelines.

Paper submitted 07/17/18; revised 01/29/19; accepted 08/13/19. Author for Correspondence: Xu Liang (email:liangxu@zju.edu.cn).
Ocean College, Zhejiang University, Hangzhou, Zhejiang 310058, China

I. INTRODUCTION

As an important fluid-structure coupling structure, pipelines are widely used in areas of various fields and vital systems, such as petroleum and chemical industry, fire-extinguishing system, irrigation system of farmland, water-supply system, biomedical field, aerospace field, hydraulic engineering, and ocean engineering field, etc. Among which, the pipelines provide a fluid link between the machine (pump) and any external fluid. The pipe fluid is excited by sources in the fluids such as pumps. The pipe wall can be excited by mechanical connections to a vibrating machine. While the machine is coupled either directly or via a flexible to pipe work which is, in turn, connected to a sub-structure by rigid or flexible supports. Potentially, many different types of wave could exist within a pipe structure and the entrained fluid. However, only those waves which dominate at low frequencies can be induced the instability, chaos and large amplitude vibration of the pipeline. Consequently, a destructive accident or rupture of the pipeline occasionally occurs. In such cases, the dominant stress waves are compressive, torsional and flexural on the pipe wall and the breathing mode traveling waves within the fluid. The pipe can be treated simply as an additional element in the vibration isolation system if structural motion is the only concern. However, the presence of the fluid leads to coupling effects between the fluid-borne and structure-borne waves as that energy conversion can occur at pipe discontinuities such as bends and joints.

As early as decades ago, some basic studies of the vibration behaviors of pipelines have been carried out by a number of scholars. Such as Ashley and Haviland (1950) analyzed the vibration characteristics of the oil pipeline across Arabia. After that, Feodos'ev (1951) and Housner (1952) were the first to study the buckling stability of pipelines supported at both ends. They used different methods to derive the linear equations of motion and drew conclusions about buckling stability. In 1955, the experimental and theoretical study of the transverse vibration of the fluid-conveying pipe was carried out by

Long (1955). He proposed that the natural frequencies of the pipe decreased with the increase of the flow velocity of the fluid. Thurman and Mote (1969) took the lead in studying the nonlinear vibration of the fluid-conveying pipes. By comparing the linear and nonlinear periods, they recognized the importance of the nonlinearity when the flow velocity was large. Païdoussis and Issid (1974) comprehensively considered factors such as gravity, external pressure, axial tension and internal loss of the structure, then developed a complete linear control equation for the pipe system. Based on this governing equation, they studied the problem of vibration instability of pipelines under various boundary conditions. In addition to the above research, in the next few decades, the research on the dynamic behavior of the fluid-conveying pipe has been carried out widely, as reviewed by Païdoussis (1998; 2004) and Ibrahim (2010; 2011) concluded. The research, related to the content of this paper, mainly involves the two aspects of nonlinear dynamics and the end configuration of the pipeline.

To date, research into the nonlinear dynamics of fluid-conveying pipes has been included in the following. Some researchers have examined the boundary conditions of the pipeline. Païdoussis and Semler (1993) used the Galerkin method to analyze the nonlinear plane dynamics of a cantilevered pipeline under intermediate spring support and revealed an interesting bifurcation behavior. Some people studied the issue of parametric resonance in pipeline systems. Panda and Kar (2008) studied the nonlinear dynamics of a pipe conveying pulsating fluid in the case of combined parameter resonance and main parameter resonance. The stability, bifurcation and response characteristics of the pipeline were studied by using the amplitude and frequency detuning of the harmonic velocity perturbation as the control parameters. Nonlinear vibration of a fluid-conveying pipe subjected to a transverse external harmonic excitation was investigated by Zhang et al. (2016) in the case with internal resonance. In the supercritical regime, the subharmonic, superharmonic, and combination resonances were examined in the presence of the internal resonance. Besides, The steady-state responses and their stability were determined. Several research methods have been developed during the research process. Setoodeh and Afrahim (2014) proposed the homotopy analysis method (HAM) to study the nonlinear vibration behavior of micro-pipes conveying fluid consisting of functionally graded materials (FGM). The results showed that the length scale parameter and the FG power-law index have significant effects on the fundamental frequency and the critical velocity of the FG micro-pipes. Wang and Ni (2008) used the differential quadrature method (DQM) to study the nonlinear dynamic behavior of a fluid-conveying curved pipe subjected to constrained motion and harmonic excitation. The results showed that the fluid-conveying curved pipe behaves as an ordinary linear system when motion is not restricted, but there is harmonic excitation. However, if the pipeline movement is constrained by three axial restrictions, the system will exhibit nonlinear dynamic phenomena. Zhang et al. (2016) developed a new method that combines the Fourier cosine series with the Runge-Kutta method, which can conveniently and effectively solve the nonlinear problems of general boundary conditions and additional springs and masses. In addition, there have also been studies of nonlinear vibration of underwater pipelines that consider current and combined wave-current (Tang et al., 2005) or at supercritical flow velocities (Yoshizawa et al., 2008).

The dynamics of fluid-conveying pipes with special-shaped components at one end were investigated in recent. Problems in bio-medicine, such as heart bypasses and cardiovascular diseases, have directed research towards cantilevered pipes. The planar dynamics of a fluid-conveying cantilevered pipe with a small mass attached at the free end was first studied, both theoretically and experimentally (Païdoussis and Semler, 1998). It has been shown that for a system without end-mass, there is only one stable periodic solution. If there is a small end-mass, the dynamics are more complex and there are different types of periodic solutions. Rinaldi and Païdoussis (2010) studied, theoretically and experimentally, the dynamics of a cantilevered flexible pipe with special end pieces. They found that different pipe-end configurations of cantilevered pipes had completely different dynamics. Research into the effect of the pipe-end configuration on the stability and critical flow velocity has also been gradually raised. Wang and Dai (2012) investigated the vibration and stability properties of fluid-conveying pipes with two symmetric elbows fitted at the downstream end, it was found that the stability of the pipeline can be greatly enhanced with this downstream elbows and the vibration frequency of the pipe can be effectively controlled by changing the angle of the elbows. Pipe-end configuration has been studied for carbon nanomaterials. Vibration and stability analyses of a Y-shaped single-walled carbon nanotube (SWCNT) embedded in viscoelastic Pasternak-based and transported nano-magnetic viscous fluids (NMF) were investigated by Arani and Zerei (2015). Their results showed that increasing the angle between the CNT center line and the downstream elbows reduced system stability. Besides, Firouz-Abadi et al. (2013) analyzed the stability of a horizontal cantilevered fluid-conveying pipe with an inclined terminal nozzle to investigate the effects of nozzle angle, nozzle aspect ratio, mass ratio and bending-to-torsional stiffness ratio on the chatter velocity of the system.

Comprehensive reviews of the nonlinear dynamic behavior of fluid-conveying pipes and the dynamics of fluid-conveying pipes with special-shaped components at one end are given in the above literature. It can be found that the existing research on the end-transformed pipelines mainly focuses on the cantilever tubes, and is mainly concerned with the natural frequencies and critical flow velocity problems, with little research into the nonlinear dynamic response. To combine the issues of nonlinear dynamic behaviors of fluid-conveying pipes and its instability characteristics sensitive to the end pieces of a fluid-conveying pipe, this paper will conduct an integrated study and discussions regarding the nonlinear dynamic response of a

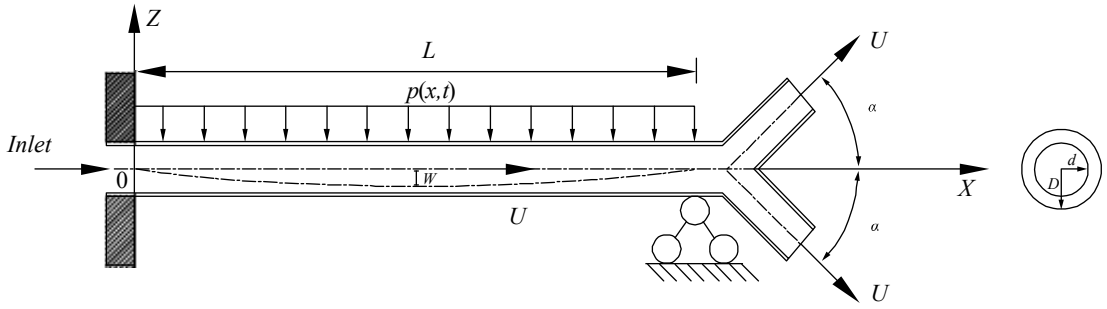

Fig. 1. Geometry of a fluid-conveying pipe with a Y-type manifold.

fluid-conveying pipe with special-type manifold under different end conditions, where the effects of related parameters in relations to the critical flow velocity and the nonlinear displacement response are involved.

II. PROBLEM DESCRIPTION

This study considers a linear elastic pipe with a Y-type manifold fitted at the downstream end. The pipe conveys an incompressible fluid with a velocity U, which is subjected to a uniform force $p(x,t)$. The geometry and the Cartesian coordinate system are shown in Fig. 1, in which the origin of the coordinate system (x, z) is considered to be located in space at the left end of the pipe. A Y-Type manifold, which is symmetrical about the X-axis, is configured at the downstream end of the pipe. The angle (α) between the central axis of the fluid-conveying pipe and the manifold varies from 0° to 90°. The pipe length is L; the cross-sectional area of the pipe is A; the inner and outer diameters of the pipe are d and D, respectively. This work will conduct an integrated study and discussions regarding the nonlinear dynamic response of a fluid-conveying pipe with a special-type manifold under different end conditions, where the effects of related parameters in relations to the critical flow velocity and the nonlinear displacement response are involved.

1. Governing differential equations

First of all, the following assumptions are made: (1) the fluid within the pipe (internal fluid) is incompressible and has a constant velocity; (2) the cross-section of the elastic pipe is uniform, and the effects of gravity, internal damping, pressurization effects, shear, torsion, and rotational inertia can be neglected; (3) the length of special-shaped manifold is small enough to be neglected; (4) the pipe is a slender beam model, and there is a geometric nonlinearity that can not be ignored during transverse vibration. As a result, the influence of the axial force caused by the axial strain during the deformation process is considered here.

Adopting the small deformation assumption and taking the pipe as an Euler-Bernoulli beam, the governing equations of motion for the fluid-conveying system are derived by using Hamilton's principle, which is defined as:

$$\int_{t_1}^{t_2} \delta(T-V)dt + \int_{t_1}^{t_2} \delta W_{nc} dt = 0 \tag{1}$$

where T is the total kinetic energy of the system; V is the potential energy of the system, consisting of the strain energy and the work done by the conservative force; W_{nc} denotes the work done by the non-conservative force.

The total kinetic energy of the fluid-conveying pipes system includes the kinetic energy of the pipe, the kinetic energy of the internal fluid and the kinetic energy of the manifold, which is represented as:

$$T = \frac{1}{2}\int_0^L m_p \left(\frac{\partial w}{\partial t}\right)^2 dx + \frac{1}{2}\int_0^L m_f \left(\left(\frac{\partial w}{\partial t} + U\frac{\partial w}{\partial x}\right)^2 + U^2\right)dx + \frac{1}{2}\int_0^L m_e \delta(x-L)\left(\frac{\partial w}{\partial t}\right)^2 dx \tag{2}$$

where: $w(x,t)$ is the deflection of the pipe; and m_p, m_f and m_e are respectively the mass per unit length of the pipe, the mass per unit length of the internal fluid and the mass of the special-type manifold. The strain energy of the system has three components, the bending strain energy, the average axial strain energy and the axial strain energy caused by the interaction of the internal flow and the manifold, described by the following equation:

$$V_s = \frac{1}{2}\int_0^L EI\left(\frac{\partial^2 w}{\partial x^2}\right)^2 dx + \frac{EA}{8L^2}\int_0^L \left(\int_0^L (\frac{\partial w}{\partial x})^2 dx\right)^2 dx + \frac{1}{2}\int_0^L F_e (\frac{\partial w}{\partial x})^2 dx \tag{3}$$

where: EI is the flexural rigidity of the pipe; EA is the tension or compression rigidity of the pipe; L is the length of the fluid-conveying pipe; and F_e is the tension exerted on the pipe due to the interaction of the internal flow and the manifold. The work done by an externally applied force $p(x,t)$ can be defined as:

$$V_f = -\int_0^L p(x,t) w dx \tag{4}$$

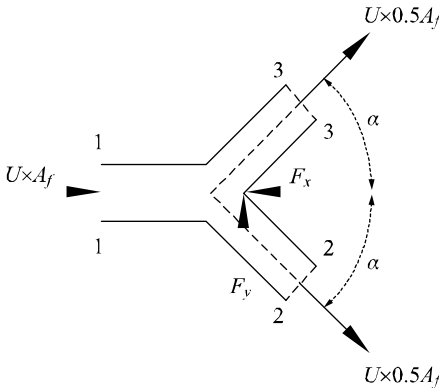

Fig. 2. Control volume of fluid at the Y-type manifold.

where $p(x,t)$ is the distributed excitation. Substituting equations (2) through (4) into Eq. (1), the following expression is derived:

$$EI\frac{\partial^4 w}{\partial x^4}+\left(m_f U^2-F_e-\frac{EA}{2L}\int_0^L(\frac{\partial w}{\partial x})^2 dx\right)\frac{\partial^2 w}{\partial x^2}+2m_f U\frac{\partial^2 w}{\partial x\partial t}$$
$$+(m_f+m_p)\frac{\partial^2 w}{\partial t^2}+m_e\delta(x-L)\frac{\partial^2 w}{\partial t^2}=p(x,t) \tag{5}$$

where x is the axial coordinate and t is time. When the fluid-conveying pipe is supported at both ends (pinned–pinned; clamped–clamped; clamped–pined), we can easily conclude that $m_e\delta(x-L)\frac{\partial^2 w}{\partial t^2}\equiv 0$. Thus the governing equation of motion for a pipe system supported at both ends is given by:

$$EI\frac{\partial^4 w}{\partial x^4}+\left(m_f U^2-F_e-\frac{EA}{2L}\int_0^L(\frac{\partial w}{\partial x})^2 dx\right)\frac{\partial^2 w}{\partial x^2}$$
$$+2m_f U\frac{\partial^2 w}{\partial x\partial t}+(m_f+m_p)\frac{\partial^2 w}{\partial t^2}=p(x,t) \tag{6}$$

The next step is thus to derive the tensile force F_e, by analyzing the control volume of fluid, as shown in Fig. 2. Fluid flows into the manifold from the pipe at section 1–1 (the cross-sectional area is A_f), while outflow from the characteristic sections 2-2 and 3-3 (each cross-sectional area is $0.5A_f$). Since we assumed that we can neglect gravity and pressurization effects, the control volume of fluid can be simplified as a jet model. The forces (F_x and F_y) of the manifold acting on the control volume of fluid can be obtained by using the steady flow momentum equation (Larock et al., 2000). The components of the momentum equation are given by:

$$F_x=(\rho\frac{Q}{2}\beta_2 U\cos\alpha+\rho\frac{Q}{2}\beta_3 U\cos\alpha)-\rho Q\beta_1 U$$
$$=m_f U^2(\cos\alpha-1) \tag{7}$$

$$F_y=(\rho\frac{Q}{2}\beta_2 U\sin\alpha-\rho\frac{Q}{2}\beta_3 U\sin\alpha)-\rho Q\beta_1\times 0=0 \tag{8}$$

where: ρ is the fluid density; Q is the volume flow rate through the pipe; U is the mean flow velocity of the transverse profile; and β_i is the compensation coefficient of momentum for each characteristic section, which is usually taken as 1.

The force (F_e) of fluid on the pipe-end piece, opposing F_x, is:

$$F_e=-F_x=-m_f U^2(\cos\alpha-1) \tag{9}$$

Substituting Eq. (9) into Eq. (6), the governing differential equation can be rewritten as:

$$EI\frac{\partial^4 w}{\partial x^4}+\left(m_f U^2\cos\alpha-\frac{EA}{2L}\int_0^l(\frac{\partial w}{\partial x})^2 dx\right)\frac{\partial^2 w}{\partial x^2}$$
$$+2m_f U\frac{\partial^2 w}{\partial x\partial t}+(m_f+m_p)\frac{\partial^2 w}{\partial t^2}=p(x,t) \tag{10}$$

2. Boundary conditions at the pipe ends

The fluid-conveying pipe is usually considered to be pinned or clamped at each end (x = 0 and x = L). Three combinations of pipe-end conditions are considered here: pinned—pinned (P–P), clamped—clamped (C–C) and clamped—pinned (C–P). The boundary conditions at the ends are as follows.

P–P, pinned (x = 0)–pinned (x = L):

$$\text{at}\quad x=0,\ w=0,\ \text{and}\ \frac{\partial^2 w}{\partial x^2}=0; \tag{11}$$

$$\text{at}\quad x=L,\ w=0,\ \text{and}\ \frac{\partial^2 w}{\partial x^2}=0; \tag{12}$$

C–C, clamped (x = 0)–clamped (x = L):

$$\text{at}\quad x=0,\ w=0,\ \text{and}\ \frac{\partial w}{\partial x}=0; \tag{13}$$

$$\text{at}\quad x=L,\ w=0,\ \text{and}\ \frac{\partial w}{\partial x}=0; \tag{14}$$

C–P, clamped (x = 0)–pinned (x = L):

$$\text{at}\quad x=0,\ w=0,\ \text{and}\ \frac{\partial w}{\partial x}=0; \tag{15}$$

$$\text{at}\quad x=L,\ w=0,\ \text{and}\ \frac{\partial^2 w}{\partial x^2}=0; \tag{16}$$

Table 1 Values of λ_1 and σ_1 for different boundary conditions.

Boundary conditions		$i=1$		$i=1$		$i=1$		$i=1$	
$\varepsilon=0$	$\varepsilon=1$	λ_1	σ_1	λ_2	σ_2	λ_3	σ_3	λ_4	σ_4
Pinned	Pinned	π	1	2π	1	3π	1	4π	1
Clamped	Clamped	4.730	0.983	7.853	1.001	10.984	1	14.137	1
Clamped	Pinned	3.927	1.001	7.069	1	10.210	1	13.352	1

3. Non-dimensionalization

The following dimensionless variables are introduced for research convenience:

$$\eta=\frac{w}{L},\varepsilon=\frac{x}{L},\tau=\sqrt{\frac{EI}{m_p+m_f}}\frac{t}{L^2},u=\sqrt{\frac{mf}{EI}}UL$$
$$\beta=\frac{m_f}{m_p+m_f},\varphi=\frac{D}{L},a=\frac{d}{D} \tag{17}$$

Eq.(9) can be written in dimensionless form as.

$$\frac{\partial^4\eta}{\partial\varepsilon^4}+(u^2\cos\alpha-\frac{8(1-a^2)}{\varphi^2(1-a^4)}\int_0^1(\frac{\partial\eta}{\partial\varepsilon})^2d\varepsilon)$$
$$\frac{\partial^2\eta}{\partial\varepsilon^2}+2\sqrt{\beta}u\frac{\partial^2\eta}{\partial\varepsilon\partial\tau}+\frac{\partial^2\eta}{\partial\tau^2}=p(\varepsilon,\tau) \tag{18}$$

The dimensionless boundary conditions are given as follows:

P–P, pinned ($\varepsilon=0$)–pinned ($\varepsilon=1$):

$$\eta(0,\tau)=0,\eta(1,\tau)=0,\frac{\partial^2\eta(0,\tau)}{\partial\varepsilon^2}=0,\frac{\partial^2\eta(1,\tau)}{\partial\varepsilon^2}=0 \tag{19}$$

C–C, Clamped ($\varepsilon=0$)–Clamped ($\varepsilon=L$):

$$\eta(0,\tau)=0,\eta(1,\tau)=0,\frac{\partial\eta(0,\tau)}{\partial\varepsilon}=0,\frac{\partial\eta(1,\tau)}{\partial\varepsilon}=0 \tag{20}$$

C–P, Clamped ($\varepsilon=0$)–Pinned ($\varepsilon=L$):

$$\eta(0,\tau)=0,\eta(1,\tau)=0,\frac{\partial\eta(0,\tau)}{\partial\varepsilon}=0,\frac{\partial^2\eta(1,\tau)}{\partial\varepsilon^2}=0 \tag{21}$$

III. SOLUTION PROCEDURE

The Galerkin method is used to discretize the infinite-dimensional pipe system, and the dimensionless displacement is:

$$\eta(\varepsilon,\tau)=\sum_{i=1}^{N}\phi_i(\varepsilon)q_i(\tau) \tag{22}$$

where: $q_i(\tau)$ are the generalized coordinates of the discretized pipe system; and $\phi_i(\varepsilon)$ are the beam eigenfunctions for the corresponding boundary conditions, given by：

$$\phi_i(\varepsilon)=k_1\cosh(\lambda_i\varepsilon)+k_2\cos(\lambda_i\varepsilon)$$
$$-\sigma_i\left[k_3\sinh(\lambda_i\varepsilon)+k_4\sin(\lambda_i\varepsilon)\right] \tag{23}$$

The values of coefficients λ_i, σ_i, and k_i are determined according to the boundary conditions of the pipe:

(a) P–P, pinned ($\varepsilon=0$)–pinned ($\varepsilon=1$):

$$\lambda_i=i\pi,k_1=k_2=k_3=0,k_4=\sigma_i=1 \tag{24}$$

(b) C–C, clamped ($\varepsilon=0$)–clamped ($\varepsilon=L$):

$$\cosh\lambda_i\cos\lambda_i=1,\sigma_i=\frac{\sinh\lambda_i+\sin\lambda_i}{\cosh\lambda_i-\cos\lambda_i},$$
$$k_1=-k_2=k_3=-k_4=1 \tag{25}$$

(c) C–P, clamped ($\varepsilon=0$)–pinned ($\varepsilon=L$):

$$\tan\lambda_i=\tanh\lambda_i,\sigma_i=\frac{\cosh\lambda_i+\cos\lambda_i}{\sinh\lambda_i+\sin\lambda_i},$$
$$k_1=-k_2=k_3=-k_4=1 \tag{26}$$

The values of coefficients λ_i and σ_i under different boundary conditions are shown in Table 1.

Substituting Eq. (22) into Eq. (18), multiplying by $\int_0^1\phi_j(\varepsilon)d\varepsilon$ and integrating from 0 to 1, yields:

$$[A]\cdot\{q\}+(u^2\cos\alpha-\frac{8(1-a^2)}{\varphi^2(1-a^4)}mm)$$
$$[B]\cdot\{q\}+2\sqrt{\beta}u[C]\cdot\{\dot{q}\}+[I]\cdot\{\ddot{q}\}=\{p\} \tag{27}$$

where:

$$[A]=\int_0^1\{\phi_j\}\cdot\{\phi_i\}^{(4)T}d\varepsilon; \tag{28}$$

$$[B]=\int_0^1\{\phi_j\}\cdot\{\phi_i\}^{(2)T}d\varepsilon; \tag{29}$$

$$[C]=\int_0^1 \{\phi_j\}\cdot\{\phi_i\}^{(1)T} d\varepsilon ; \tag{30}$$

$$[I]=\int_0^1 \{\phi_j\}\cdot\{\phi_i\}^{T} d\varepsilon ; \tag{31}$$

$$\{q\}=\left[q_1(\tau),q_2(\tau),\cdots,q_i(\tau)\right]^T ; \tag{32}$$

$$\{\dot{q}\}=\left[\dot{q}_1(\tau),\dot{q}_2(\tau),\cdots,\dot{q}_i(\tau)\right]^T ; \tag{33}$$

$$\{\ddot{q}\}=\left[\ddot{q}_1(\tau),\ddot{q}_2(\tau),\cdots,\ddot{q}_i(\tau)\right]^T ; \tag{34}$$

$$\{p\}=\int_0^1 \{\phi_j\}p(\varepsilon,\tau)d\varepsilon ; \tag{35}$$

$$mm=\int_0^1\left[\sum_{i=1}^{N}\phi_i^{(1)}(\varepsilon)q(\tau)\right]^2 d\varepsilon ; \tag{36}$$

For simplicity, Eq. (27) can be expressed as:

$$[I]\{\ddot{q}\}+[S]\{\dot{q}\}+[R]\{q\}=\{p\} \tag{37}$$

where:

$$[S]=2\sqrt{\beta}u[C]; \tag{38}$$

$$[R]=[A]+(u^2\cos\alpha-\frac{8(1-a^2)}{\phi^2(1-a^4)}mm)[B]; \tag{39}$$

Eq.(37) shows a second-order ordinary differential system of nonlinear equations. There are many ways to solve this problem. In this paper, a four order Runge-Kutta method is used to solve it. After getting the solution of Eq.(37), the dimensionless deflection of the pipe can be obtained by Eq.(22).

IV. RESULTS AND DISCUSSIONS

In this part, based on the formulations obtained above, the numerical solutions of the nonlinear dynamic response of a fluid-conveying pipe with special-type manifold are conducted and discussed. Matlab software is used to program the calculations and solve the equations. We analyze the model as follows. First, the numerical results are compared with the existing literature to verify the correctness and accuracy of our method. Second, the critical flow velocity of a fluid-conveying pipe with Y-type manifold is discussed. Third, the contribution of different mode to the dimensionless deflection is discussed. Fourth, the effects of different end conditions on pipe dimensionless nonlinear displacement are analyzed. Fifth, the effect of the angle(α) between the central axis of the fluid-conveying pipe and the manifold is discussed. Sixth, the effects of the aspect ratio (L/D) and fluid velocity are analyzed. Finally, the influence of different parameters on the nonlinearity of the pipe is discussed by comparing the linear and nonlinear transient dimensionless displacement responses. In the following sections, if not otherwise specified, the parameters listed in Table 2 are used.

Table 2 Values of physical parameters.

Parameters	Items	Values
E	Elastic modulus (GN/m^2)	210
L	Length of the pipe (m)	15
D	External diameter (m)	0.25
d	Internal diameter (m)	0.125
α	The angle of the manifold (°)	45
ρ_p	Pipe density (kg/m^3)	7800
ρ_f	Internal fluid density (kg/m^3)	870
u	Dimensionless fluid velocity	1
$p(\varepsilon,\tau)$	Dimensionless distributed excitation	0.06 π

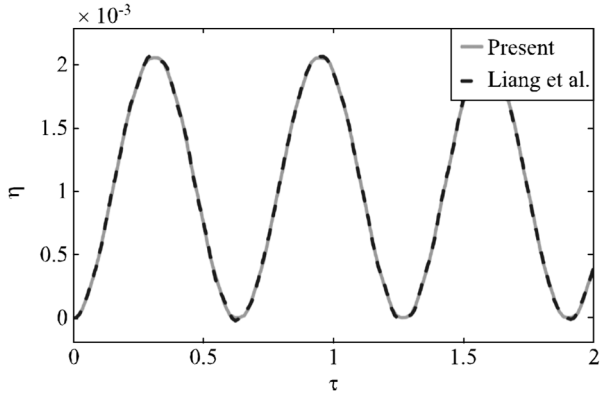

Fig. 3. Dimensionless time histories of the dimensionless pipe deflection at the midpoint.

1. Validation

In order to verify the correctness and accuracy of the numerical method proposed in this study, the results are compared with those in the existing literature. In the verification process, all material parameters and geometric parameters are consistent with the cited references. A P–P fluid-conveying pipe is considered here. The dimensionless time histories of the dimensionless pipe deflection at the midpoint ($\varepsilon = 0.5$) are plotted in Fig. 3. As is demonstrated in Fig. 3 that results generated by the present method agree well with those of Liang's (Liang et al., 2018).

Table 3 shows the first four frequencies of the pipe with different end conditions for $u = 0$. The relative error between the present results and the exact results from Ni et al. (Ni et al., 2011) and Thomson (Thomson., 1988) is within 0.033%. The above shows the correctness and high precision of the present method.

Table 3 Dimensionless natural frequency of the pipe with different end conditions for $u = 0$.

	End conditions	ω_1	ω_2	ω_3	ω_4
P–P	Present	9.8696	39.4784	88.8264	157.9173
	Exact solution (Thomson, 1988; Ni et al., 2011)	9.8696	39.4784	88.8264	157.9173
	Relative error	0.0000%	0.0000%	0.0000%	0.0000%
C–P	Present	15.4213	49.9708	104.2441	178.2759
	Exact solution (Thomson, 1988; Ni et al., 2011)	15.4182	49.9649	104.2477	178.2697
	Relative error	0.0201%	0.0118%	0.0035%	0.0035%
C–C	Present	22.3729	61.6696	120.8642	199.8547
	Exact solution (Thomson, 1988; Ni et al., 2011)	22.3733	61.6728	120.9034	199.8594
	Relative error	0.0018%	0.0052%	0.0324%	0.0024%

Table 4 Dimensionless critical flow velocities with increasing angles under end conditions P–P, C–C and C–P.

α/π	u_{cr}		
	P–P	C–C	C–P
0	3.15	6.31	4.49
0.05	3.17	6.35	4.52
0.10	3.23	6.47	4.61
0.15	3.33	6.69	4.76
0.20	3.50	7.02	4.99
0.25	3.74	7.51	5.34
0.30	4.10	8.23	5.86
0.35	4.67	9.37	6.67
0.40	5.66	11.35	8.08
0.45	7.95	15.95	11.35

2. Critical flow velocity

Natural frequencies and critical flow velocities are an essential part of a pipeline system. In this section, the critical flow velocities of a fluid-conveying pipe with special-type manifold under the three boundary conditions (P–P, C–C and C–P) are examined. For these three sets of boundary conditions, the stability of the pipe is mainly determined by the first-order mode, so the critical flow velocities examined here refer to the flow velocities when the first-order mode is about to destabilize. In the research process, 10 different angles between the central axis of the fluid-conveying pipe and the manifold were used.

Table 4 shows the evolution of dimensionless critical flow velocities with increasing angles for boundary conditions P–P, C–C and C–P, respectively. When all other factors are the same, the C–C pipe has the largest dimensionless critical flow velocity, followed by the C–P pipe. The dimensionless critical flow velocity is the smallest for the P–P pipe. In addition, it can be found that as the angle increases, the dimensionless critical flow velocity of the fluid-conveying pipe rises up significantly for all three end conditions. Therefore, the configuration of the special-type manifold can improve the stability of the pipe.

3. Modal separation analyses

This part analyzes the influence of first to fourth-order modes on the dimensionless deflection of the fluid-conveying pipe with a special-type manifold. The boundary condition is P—P and the manifold angle $\alpha = 45°$.

Dimensionless time histories and spectral analyses at two selected positions ($\varepsilon = 0.2$ and $\varepsilon = 0.5$) are plotted in Fig. 4 and Fig. 5. The left column shows the dimensionless time histories in the interval $\tau \in [0,3]$, while the right column is spectral analysis based on fast Fourier transform algorithm (FFT). The dimensionless displacement for mode 1 has the same scale as the original one, and the displacement curve of mode 1 has a similar shape to the original one. However, the other modes differ from the original both in terms of scale and shape. We conclude that the first mode is the most important in the dimensionless displacement of the pipe, which is also supported by the spectral analysis.

4. Effects of the different end conditions

This section analyzes the influence of three different boundary conditions (P–P, C–C and C–P) on the dimensionless nonlinear deflection of the fluid-conveying pipe with a Y-type manifold. A four-order mode truncation is adopted in the Galerkin method to ensure the convergence and accuracy of the results. The dimensionless time histories of the nonlinear displacement at the midpoint ($\varepsilon = 0.5$) of the pipe under different end conditions are shown in Fig. 6.The fluid-conveying pipe with Y-type manifold for the P–P end condition has the largest peak displacement, followed by C–P, and the vibration amplitude of the pipe for C–C is the smallest. The dimensionless peak displacement of the pipe increases with an increase in the total number of degrees of freedom at the ends.

5. Effects of the manifold angle (α)

This section examines the response of the pipe to change in the angle between the central axis of the fluid-conveying pipe and the manifold. Different angles (0°, 30°, 45°, 60°, and 90°) are used. Two indexes of d_{ai} and p_{ai} are introduced to quantitatively describe the influence of the manifold angle on the peak deflection and period of nonlinear displacement response, such that:

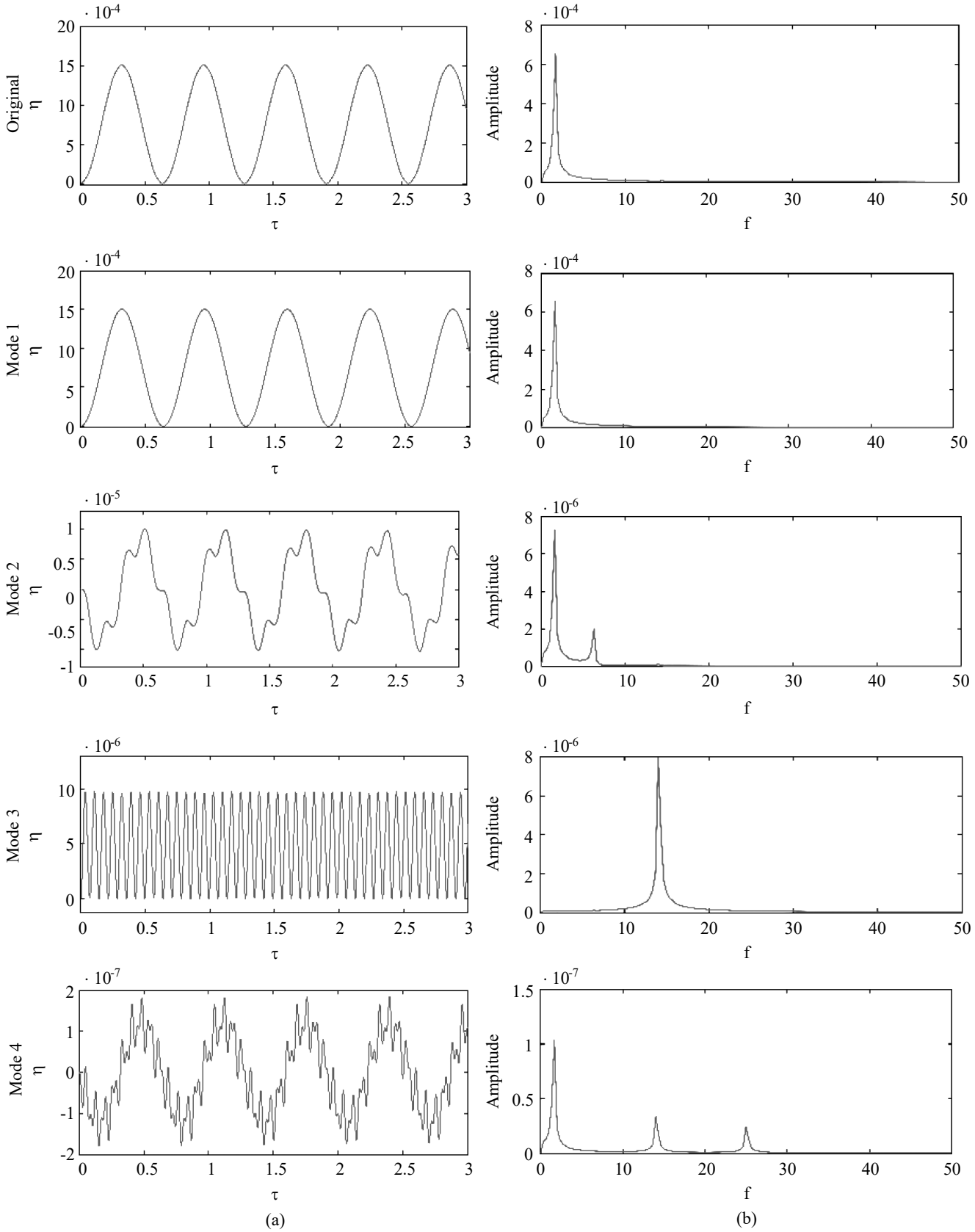

Fig. 4. (a) Mode separation of dimensionless time histories of dimensionless displacement in a dimensionless time interval $\tau \in [0,3]$ at the point $\varepsilon = 0.2$; (b) Spectral analysis of (a).

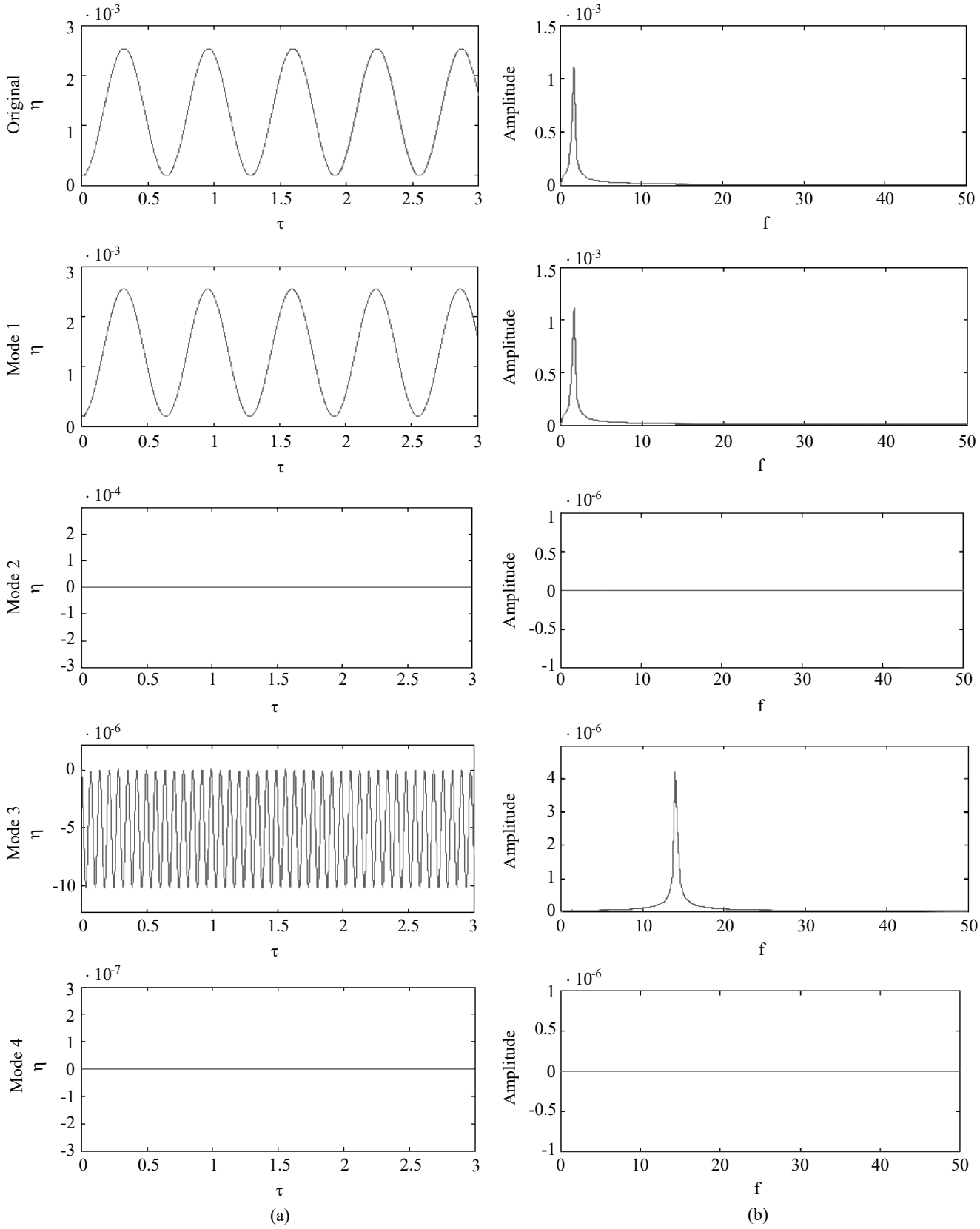

Fig. 5. (a) Mode separation of dimensionless time histories of dimensionless displacement in a dimensionless time interval $\tau \in [0,3]$ at the point $\varepsilon = 0.5$; (b) Spectral analysis of (a).

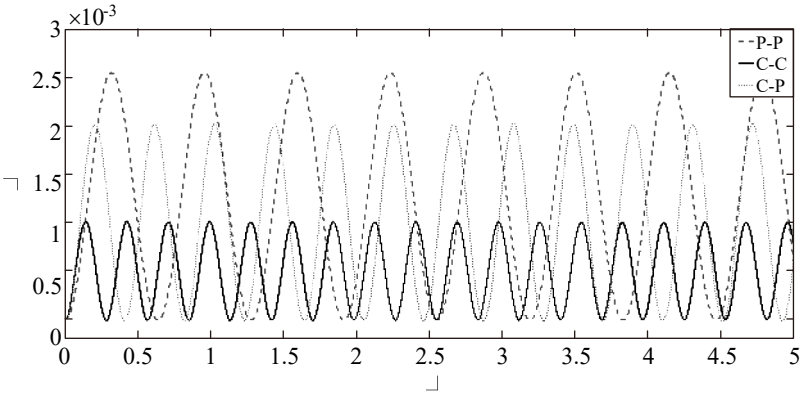

Fig. 6. Dimensionless time histories of dimensionless displacement in a dimensionless time interval $\tau \in [0,5]$, at the midpoint ($\varepsilon = 0.5$).

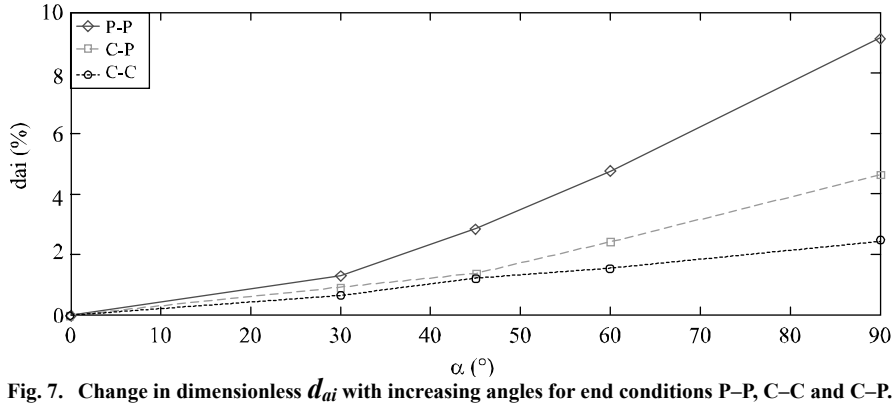

Fig. 7. Change in dimensionless d_{ai} with increasing angles for end conditions P–P, C–C and C–P.

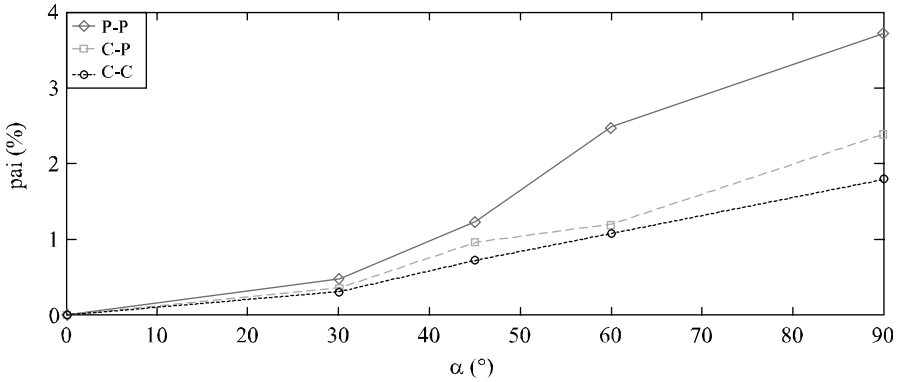

Fig. 8. Change in dimensionless p_{ai} with increasing angles for end conditions P–P, C–C and C–P.

$$d_{ai} = \left| \frac{d_{without-manifold} - d_{with-manifold}}{d_{without-manifold}} \right|, \qquad p_{ai} = \left| \frac{p_{without-manifold} - p_{with-manifold}}{p_{without-manifold}} \right| \tag{40}$$

where: d_{ai} is the deflection angle index; p_{ai} is the period angle index; $d_{without\text{-}manifold}$ is the dimensionless peak deflection of pipe without the manifold; $d_{with\text{-}manifold}$ is the dimensionless peak deflection of pipe with the manifold; $p_{without\text{-}manifold}$ is the dimensionless period of pipe without the manifold; and $p_{with\text{-}manifold}$ is the dimensionless period of pipe with the manifold. The influence of manifold angle on displacement response is positively related to the values of the two indexes.

Fig. 7 and Fig. 8 show change in d_{ai} and p_{ai} with increasing angles for end conditions P–P, C–C and C–P. As the angle increases, the dimensionless peak deflection and dimensionless period of the pipe decreases. This change is most obvious for P–P and least obvious for C–C. The result shows that the

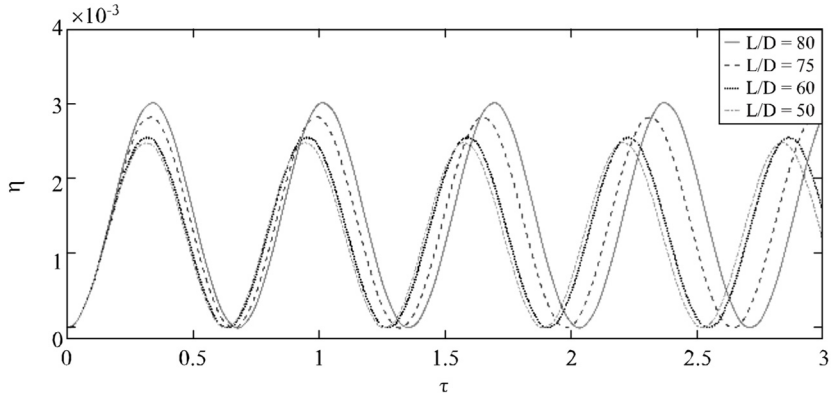

Fig. 9. Time histories of displacement at the midpoint ($\varepsilon = 0.5$) for different aspect ratio, for end condition P–P.

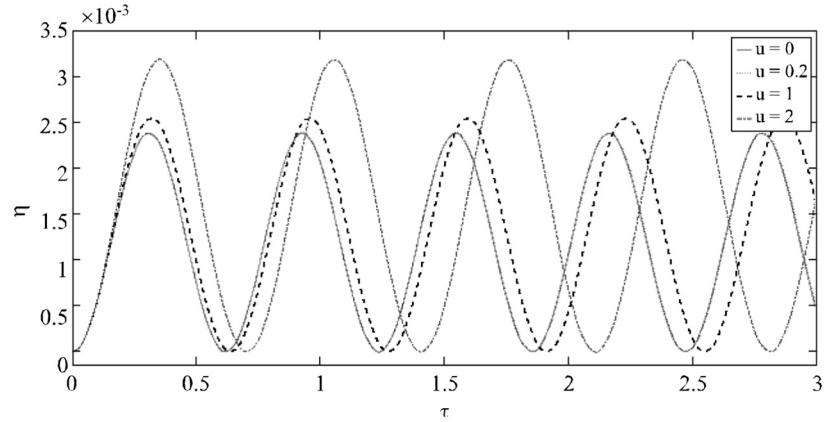

Fig. 10. Dimensionless time histories of dimensionless displacement at the midpoint ($\varepsilon = 0.5$) for different dimensionless velocity, for end condition P–P.

configuration of the Y-shaped manifold enhances the stability of the pipe to some extent. According to Eq. (8), the change in the angle affects the axial tensile force, which changes the dimensionless displacement response.

6. The effects of aspect ratio and fluid velocity

This section discusses the influences of the aspect ratio (L/D) on the nonlinear behavior of the fluid-conveying pipe with a Y-type manifold. Different values are used for the aspect ratio (L/D = 50, 60, 75, and 80). Fig. 9 shows that the dimensionless peak deflection rises up with the increase in the aspect ratio.

Fig. 10 shows the dimensionless time histories of the nonlinear displacement with different dimensionless flow velocity (u = 0, 0.2, 1 and 2). The results show that when the dimensionless velocity is small (u = 0 or 0.2), dimensionless peak deflection is insensitive to the dimensionless velocity. When the dimensionless velocity is relatively large (u = 1 or 2), the dimensionless peak deflection increases with the increase in the dimensionless velocity.

7. Effects of parameters on the nonlinearity

This section discusses the effects of the end condition, aspect ratio, and the angle between the central axis of the fluid-conveying pipe and the manifold on nonlinearity by comparing the linear and nonlinear dimensionless time histories. In order to quantitatively assess the strength of nonlinearity, the following two indexes, for deflection and period, are introduced.

$$d_{ni} = \left| \frac{d_{linear} - d_{nonlinear}}{d_{linear}} \right|, \qquad p_{ni} = \left| \frac{p_{linear} - p_{nonlinear}}{p_{linear}} \right| \tag{41}$$

where d_{ni} is the deflection nonlinearity index; p_{ni} is the period nonlinearity index; d_{linear} is the linear dimensionless peak deflection; $d_{nonlinear}$ is the nonlinear dimensionless peak deflection; p_{linear} is the linear dimensionless period; and $p_{nonlinear}$ is the nonlinear dimensionless period. The greater the d_{ni} and p_{ni} values, the more significant the nonlinearity of the pipeline system.

To begin with, the effect of the end conditions on nonlinearity is studied. From the data in Table 5, it is clear that the two indexes of d_{ni} and p_{ni} are fairly small for C–C (0.44% and 0.35%), while those for P–P are significantly greater (11.75% and 9.72%). This indicates that the nonlinearity effect of pipeline

Table 5. Nonlinearity indexes d_{ni} and p_{ni} versus end conditions.

End condition	d_{ni} (%)	p_{ni} (%)
C–C	0.44	0.35
C–P	4.14	3.83
P–P	11.75	9.72

Table 6. Nonlinearity indexes d_{ni} and p_{ni} versus manifold angle α for end condition P-P.

α (°)	d_{ni} (%)	p_{ni} (%)
0	12.69	9.85
30	12.30	9.67
45	11.75	9.42
60	11.13	9.20
90	9.78	7.94

Table 7. Nonlinearity indexes d_{ni} and p_{ni} versus aspect ratio L/D for end condition P-P.

L/D	d_{ni} (%)	p_{ni} (%)
50	8.53	8.95
60	11.75	10.18
75	19.60	14.45
80	23.80	20.05

increases with the increase in the total number of degrees of freedom at the ends. Nonlinearity is sensitive to the end conditions.

The value of the manifold angle α is varied in the range of [0°, 90°]. Table 6 shows that the values of d_{ni} and p_{ni} decrease as α increases, but the ranges of the decrease are smaller (2.91% and 1.91%). This shows that there is an inverse correlation between the manifold angle and nonlinearity, but the influence is relatively insignificant.

Finally, the effect of aspect ratio on nonlinearity is examined. The results are shown in Table 7. There is a positive correlation between the nonlinearity of the pipeline system and the aspect ratio.

V. CONCLUSIONS

In this study, We studied the nonlinear dynamic response of a fluid-conveying pipe with a Y-type manifold for three end conditions, P–P, C–C and C–P. Using Hamilton's principle and the momentum equations for a steady flow, the governing differential equations were derived and solved using the Galerkin method and the Runge-Kutta methods with truncation order 4. The numerical results were compared with the existing literature and showed in good agreement.

Parametric analyses of the nonlinear dynamic response were conducted. Among which, the parameters such as the angle of the manifold, the aspect ratio, the end constraints of the pipe and the flow velocity are taken into consideration. It was concluded that : (1) the dimensionless critical flow velocity of the fluid-conveying pipe rises up significantly and the dimensionless peak deflection decreases as the angle between the central axis of pipe and manifold increases; (2) the dimensionless peak deflection of the pipe goes up as the aspect ratio increases; (3) the dimensionless peak displacement of the pipe increases with an increase in the total number of degrees of freedom at the ends; (4) when the dimensionless velocity is small, dimensionless peak deflection is insensitive to the dimensionless velocity, but when it is large, the dimensionless peak deflection rises up with the increase of the dimensionless velocity; (5) the nonlinear behavior of the pipe is mainly dominated by the first-order mode; (6) the nonlinearity of the pipe is positively correlated with the aspect ratio and the total number of degrees of freedom at the ends, and this effect is significant. However, there is a non-significant inverse correlation between the manifold angle and nonlinearity.

ACKNOWLEDGMENTS

The authors gratefully acknowledge the financial support provided by the Fundamental Research Funds for the Central Universities (2016QNA4035), and by the National Natural Science Foundation of China (Nosd51379185, 51679214).

REFERENCES

Ashley, H. and G. Haviland (1950). Bending vibrations of a pipe line containing flowing fluid. Applied Mechanics 17, 229-232.

Feodos'Ev, V. P. (1951). Vibrations and stability of a pipe when liquid flows through it. Inzhenernyi Sbornik 10, 169-170.

Firouz-Abadi, R. D., A. R. Askarian and M. Kheiri (2013). Bending-torsional flutter of a cantilevered pipe conveying fluid with an inclined terminal nozzle. Journal of Sound and Vibration 332, 3002-3014.

Ghorbanpour Arani, A. and M. Sh. Zarei (2015). Nonlocal vibration of Y-shaped CNT conveying nano-magnetic viscous fluid under magnetic field. Ain Shams Engineering Journal 6, 565-575.

Housner, G. W. (1952). Bending vibrations of a pipe line containing flowing fluid. Journal of Applied Mechanics 19, 205-208.

Ibrahim, R. A. (2010). Overview of mechanics of pipes conveying fluids. Part I: Fundamental studies. Journal of Pressure Vessel Technology 132(3).

Ibrahim, R. A. (2011). Mechanics of pipes conveying fluids-part II: applications and fluidelastic problems. Journal of Pressure Vessel Technology 133(2).

Larock, B. E., R. W. Jeppson and G. Z. Watters (2000). Hydraulics of pipeline systems. Crc Press, Boca Raton.

Liang, X., X. Zha, X. Jiang, L. Z. Wang, J. X. Leng and Z. Cao (2018). Semi-analytical solution for dynamic behavior of a fluid-conveying pipe with different boundry conditions. Ocean Engineering 163, 183-190.

Long, R. H. J. (1955). Experimental and theoretical study of transverse vibration of a tube containing flowing fluid. Journal of Applied Mechanics 22, 65-68.

Ni, Q., Z. L. Zhang and L. Wang (2011). Application of the differential transformation method to vibration analysis of pipes conveying fluid. Applied mathematics and computation 217, 7028-7038.

Païdoussis, M. P. and C. Semler (1993). Nonlinear Dynamics of a Fluid-Conveying Cantilevered Pipe with an Intermediate Spring Support. Journal of Fluids and Structures 3, 269-298.

Païdoussis, M. P. and C. Semler (1998). Non-linear dynamics of a fluid-con-

veying cantilevered pipe with a small mass attached at the free end. Journal of Non-Linear Mechanics 1, 15-32.

Païdoussis, M. P. (1998). Fluid-Structure Interactions: Slender Structures and Axial Flow. Academic Press, London, UK.

Païdoussis, M. P. (2004). Fluid-Structure Interactions: Slender Structures and Axial Flow. Academic Press, London, UK.

Païdoussis, M. P. and N. T. Issid (1974). Dynamic stability of pipes conveying fluid. Journal of Sound and Vibration 33, 267-294.

Panda, L. N. and R. C. Kar (2008). Nonlinear dynamics of a pipe conveying pulsating fluid with combination, principal parametric and internal resonances. Journal of Sound and Vibration 309, 375-406.

Rinaldi, S. and M. P. Païdoussis (2010). Dynamics of a cantilevered pipe discharging fluid, fitted with a stabilizing end-piece. Journal of Fluids and Structures 26, 517-525.

Setoodeh, A. R. and S. Afrahim (2014). Nonlinear dynamic analysis of FG micro-pipes conveying fluid based on strain gradient theory. Composite Structures 116, 128-135.

Tang, Y. G., J. Y. Gu, J. L. Zuo and J. Q. Min (2005). Nonlinear dynamics response of casing pipe under combined wave-current. Applied Mathematics and Mechanics (English Edition) 8, 1040-1046.

Thomson, and T. William (1988). Theory of vibration with applications. Unwin Hyman Ltd, London.

Thurman, A. L. and C. D. Mote (1969). Nonlinear oscillation of a cylinder containing a flowing fluid. ASME Journal of Engineering for Industry 4, 1147-1155.

Wang, L. and H. L. Dai (2012). Vibration and enhanced stability properties of fluid-conveying pipes with two symmetric manifold fitted at downstream end. Archive of Applied Mechanics 82, 155-161.

Wang, L. and Q. Ni (2008). Nonlinear dynamics of a fluid-conveying curved pipe subjected to motion-limiting constraints and a harmonic excitation. Journal of Fluids and Structures 309, 375-406.

Yoshizawa, M., T. Suzuki and M. Takayanagi (2008). Nonlinear lateral vibration of a fluid-conveying pipe with end mass. Jsme International Journal 3, 652-661.

Zhang, T., H. Ouyang, Y. O. Zhang and B.L. Lv (2016). Nonlinear dynamics of straight fluid-conveying pipes with general boundary conditions and additional springs and masses. Applied Mathematical Modelling 40, 7880-7900.

Zhang, Y., H Feng and L. Chen (2016). Supercritical Nonlinear Vibration of a Fluid-Conveying Pipe Subjected to a Strong External Excitation. Shock and Vibration 2016, 1-21.